Boundaries, interfaces, point defects, and strain as impediments to thermal transport in nanostructures

S. Mei,[1] C. J. Foss,[2] L. N. Maurer,[1,3] O. Jonasson,[1] Z. Aksamija,[2] and I. Knezevic[1]
[1]University of Wisconsin – Madison, Madison, Wisconsin, USA
[2]University of Massachusetts – Amherst, Amherst, Massachusetts, USA
[3]Sandia National Laboratories, Albuquerque, New Mexico, USA
Contact email: iknezevic@wisc.edu

***Abstract* — The ability to grow heterostructures with high-quality interfaces brings great flexibility to the design and development of modern electronic and optoelectronic devices. While nearly perfect from an electronic standpoint, these interfaces are exceedingly disruptive to thermal transport and are a major contributor to anisotropic heat conduction and localized heating. Doping, alloying, and strain — all commonly employed when tailoring the electronic and optical properties of heterostructures — are also highly detrimental to the transport of phonons, the dominant carriers of heat in semiconductors. From the theoretical standpoint of phonon dynamics in disordered systems, we discuss the present understanding of nanoscale thermal transport and its profound sensitivity to any deviation from single-crystallinity. The roles that boundaries, interfaces, point defects, and strain play in thermal transport and localized heating are illustrated on several examples of semiconductor nanostructures, such as nanowires, thin films, superlattices, and quantum cascade lasers.**

***Index Terms* — Phonons, heating, thermal conductivity, quantum cascade lasers, superlattices, nanowires, semiconductor device reliability, semiconductor nanostructures.**

I. Introduction

Thermal transport is of great importance for the operation of modern nanoscale electronic and optoelectronic devices [1,2]. In semiconductors, heat conduction is dominated by the lattice [3]. Bulk tetrahedrally bonded semiconductors have high lattice thermal conductivities, thanks to the strong sp^3 bonds and relatively low atomic masses. However, thermal transport in semiconductor nanostructures and devices is strongly affected by the existence of interfaces between different materials, point defects (e.g., alloy atoms or dopants), and strain. Considering that advanced fabrication techniques [4,5] routinely rely on heterostructuring, doping, alloying, and the growth of intentionally strained layers in order to achieve desired electronic or optical device behavior, it becomes important to understand the associated degradation in thermal conduction, which brings about exacerbated lattice heating and hotspot formation, and adversely affects device reliability [6-8].

The work at UW-Madison was supported by the U.S. Department of Energy (Office of Basic Energy Sciences, Division of Materials Sciences and Engineering, Physical Behavior of Materials Program), Award DE-SC0008712. The work was performed using the resources of the UW-Madison Center for High Throughput Computing (CHTC). The work at UMass used the Extreme Science and Engineering Discovery Environment (XSEDE) [9], supported by NSF ACI-1053575.

In this paper, we overview the current understanding of how various types of disorder affect thermal transport in common semiconductor nanostructures and devices. Specifically, we discuss the signatures of thermal conductivity degradation due to different types of disorder in group III-V and group IV semiconductor nanostructures. Finally, we focus on the quantum cascade laser (QCL) as an example of a device with several types of disorder. We analyze the heat flow patterns and the effects of localized heating on the QCL optical and electronic performance.

II. Disordered Boundaries: Thermal Transport in Nanowires, Nanoribbons, and Nanomembranes

Phonons, the quanta of lattice waves, are the dominant carriers of heat in semiconductors and their nanostructures Semiconductor structures of different dimensionality – nanowires, nanoribbons, membranes, and superlattices – are important for applications such as thermoelectric active cooling and energy harvesting, as well as for thermal management of electronic and optoelectronic devices. Therefore, it is imperative to accurately predict thermal transport in these systems. However, theoretical understanding of phonon dynamics in nanostructures with a significant degree of disorder is far from complete.

A. Semiclassical phonon transport in rough Si nanowires

One prominent open problem is the unexpectedly low thermal conductivity of very rough silicon nanowires (NWs) [10-13]. Early measurements of thermal conductivity on vapor-liquid-solid (VLS)-grown NWs [2] showed thermal conductivities an order of magnitude lower than the bulk value, but this reduction could be explained simply within the diffusive-transport framework [14]: the rough surface is described by a specularity parameter, p, which is the probability that a phonon would reflect specularly upon impact; complete randomization of phonon momentum yields the so-called diffusive or Casimir limit (p=0). Indeed, thermal transport in relatively smooth NWs is well described using the relaxation-time approximation and the model of partially or completely diffuse surface scattering [2, 15].

In contrast, the thermal conductivities measured on electrolessly etched [11] or intentionally roughened VLS-grown [13] NWs are far below the diffusive limit and have values similar to amorphous materials. While a number of different theoretical approaches can produce thermal

conductivities below the diffusive limit, few get thermal conductivities that are as low as experimentally observed. There is general agreement that pronounced roughness leads to the drastic thermal conductivity reduction in very rough Si NWs, but there is no consensus on the specific mechanism.

In most nanostructures and at temperatures that are not too low, phonon transport is diffusive or at the very least quasiballistic [16,17], so phonons obey the phonon Boltzmann transport equation (PBTE). The PBTE can be solved via deterministic techniques, with the collision operator treated either in the relaxation-time approximation [18,19] or iteratively [20]; alternatively, the PBTE can be solved via a stochastic ensemble Monte Carlo technique [17,21-23]. Modern transport simulations based on the PBTE use phonon-phonon scattering rates from first principles [20].

We considered room-temperature thermal transport in rough Si nanowires of dimensions that are directly accessible in experiment (20-70 nm). The real-space random rough boundaries were generated according to a given autocorrelation function. Figure 1 presents an exponentially correlated boundary, which is a good approximation for the experimentally observed profile on intentionally roughenend NWs [13]. The phonon reflects specularly at the point of impact. For simplicity, we assumed the nanowire is surrounded by air; in experiment, a thin native oxide likely affects experimental results [24].

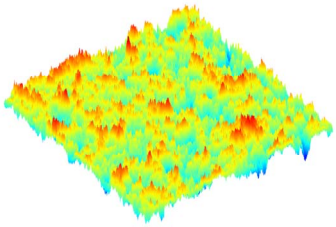

Figure 1. A rough surface with exponential autocorrelation function. Reprinted with permission from Ref. [21], copyright AIP 2015.

Recently, we employed semiclassical phonon Monte Carlo simulation and calculated ultralow thermal conductivities (Fig. 2) in Si NWs with real-space, rough surfaces (Fig. 1) of rms heights and correlation lengths similar to experiment [21]. This work showed that coherent transport is not necessary for ultralow thermal conductivity, and universal features in scaling with the width and geometric mean free path are revealed when rough NWs are considered as chaotic cavities [21]. The results stem from a number of phonon Monte Carlo (PMC) simulation of thermal transport in a rough Si nanowire with a square cross section and side edge of 70 nm, very similar to those measured in Ref. [13]. The black solid line denotes 40 W/m.K, the diffusive (Casimir) limit of thermal conductivity for the wires of this cross section. Clearly, it is not difficult to obtain thermal conductivities below the Casimir limit. Exponentially correlated surfaces have many small-scale features and scatter phonons of a variety of wavelengths.

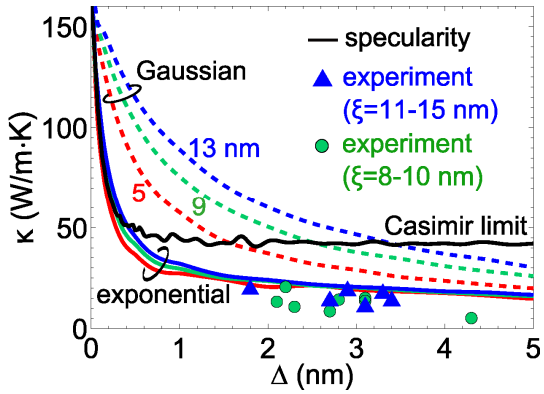

Figure 2. Thermal conductivity κ versus rms roughness Δ for 70-nm-wide SiNWs with different correlation lengths, ξ, and autocorrelation functions of the surface roughness. The symbols are experimental values [13]. Phonon Monte Carlo (PMC) results with real-space exponential (solid curves) and Gaussian (dashed curves) surfaces are presented for the correlation lengths of 5 nm (red), 9 nm (green), and 13 nm (blue). Thermal conductivity calculated by PMC with a specularity parameter (black solid) tends to the diffusive Casimir limit. Reprinted with permission from [21], copyright AIP 2015.

B. Semiclassical phonon transport in silicon-on-insulator (SOI) nanomembranes

By solving the phonon Boltzmann transport equation in the relaxation-time approximation, we investigate the sensitivity of thermal conduction in thin SOI membranes to the surface crystalline orientation, boundary roughness features, and the direction of heat flow. We calculate the full thermal conductivity tensor in (001), (011), and (111) silicon nanomembranes with thicknesses ranging from 5 to 100 nm. The calculation employs the full phonon dispersion and the Boltzmann transport equation, including three-phonon and isotope scattering, as well as a momentum-dependent boundary scattering model. The interplay between strong boundary scattering in SOI membranes and the anisotropy in the phonon dispersions results in thermal conduction that strongly depends on the surface orientation and exhibits marked in-plane vs out-of-plane anisotropy, as well as some in-plane anisotropy for low-symmetry surface orientations. For all nanomembrane surface orientations, the thermal conductivity tensor has an out-of-plane eigenvector, corresponding to the minimal eigenvalue that represents the intrinsic out-of-plane thermal conductivity of the membrane.

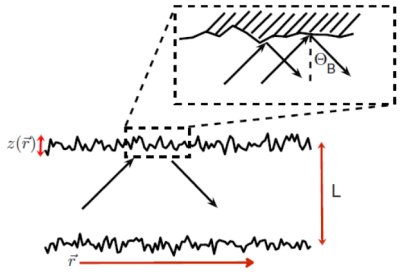

Figure 3. Schematic of a silicon nanomembrane of thickness L, showing a lattice wave scattering from the rough boundary. The phases of the waves reflected from different points on the boundary differ by amounts that depend on the local surface roughness height z and the angle between the phonon momentum **q** and the boundary surface normal of the idealized smooth surface. Reprinted with permission from Ref. [18], copyright APS 2010.

In-plane thermal conductivity is overall highest along the [100] direction on (011) SOI. There is a slight anisotropy of the in-plane conductivity on (011) SOI, which becomes more pronounced at low temperatures (i.e., long phonon mean free paths). The lowest in-plane conductivity is observed in (001) SOI due to the very strong scattering of the highly anisotropic TA modes with (001) surfaces (see Fig. 4). The room-temperature in-plane conductivities in (011) and (001) nanomembranes with thicknesses around 10 nm differ by a factor of 2. This ratio can get much higher with increased prominence of boundary scattering, i.e., with lower temperatures, intentionally roughened surfaces, or in very thin samples. We conclude that, for applications that require good thermal conduction such as in digital electronics, heating will be minimized in SOI devices if the channel is oriented as [100]/(011). In contrast, for thermoelectric applications where low thermal conductivity is needed, the best starting points are likely to be nanostructures with as many {001} facets as possible to promote the boundary scattering of TA modes, such as in etched rectangular [100] nanowires with (001) and (010) facets.

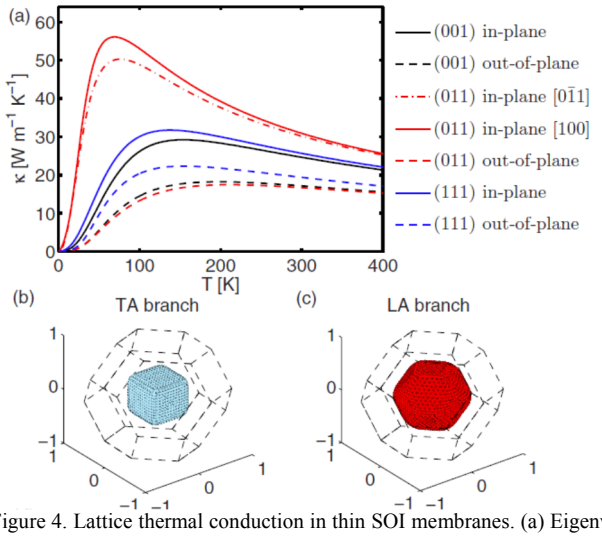

Figure 4. Lattice thermal conduction in thin SOI membranes. (a) Eigenvalues of the thermal conductivity tensor for a 20-nm-thick SOI with rms surface roughness =0.45 nm. Maximal in-plane thermal conductivity eigenvalue is along [100] on (011) SOI and it is minimal on (001) SOI due to the very strong scattering of TA modes from 001 boundaries, as described in the text. (b) and (c) Energy isosurfaces for (b) TA and (c) LA modes in silicon; dashed lines denote the Brillouin-zone shape. The TA constant-energy surfaces are boxlike with box faces perpendicular to the <001> directions. The LA mode energy isosurfaces have faces perpendicular to <111> and <001> directions. Reprinted with permission from [18], copyright APS 2010.

C. Thermal transport in nanoribbons in the elastic-solid limit

Phonon-surface scattering is inherently not specular. Even at a smooth surface, a single phonon can scatter into one of several outgoing phonons of different modes, a phenomenon known as mode conversion. At smooth surfaces, bulk phonons (longitudinal and transverse) can be converted only to other bulk phonons. Structures with free surfaces support Rayleigh surface waves (Fig. 5) [25,26], so bulk modes can also convert to Rayleigh waves at rough [27] or otherwise disordered free surfaces. Rayleigh waves are slower than bulk modes [28] and have fairly long lifetimes even in the presence of disorder [29].

Understanding Rayleigh waves is important for modeling thermal transport in modern nanostructures [2] because Rayleigh waves concentrate energy near the surface, where disorder is often high [11,13,21]. Yet, relatively little is known about the effects of Rayleigh waves and surface modes in general on phonon thermal transport. In spite of considerable recent interest in phonon transport at the nanoscale [2], surface modes in disordered nanostructures have received limited attention. Nakayama [30] identified Rayleigh wave mode conversion as a cause of diffuse surface scattering, which is important to many phonon-surface scattering models [14]. Using molecular dynamics, Kang and Estreicher [31] showed that mode conversion between bulk modes and confined surface modes can lead to "phonon trapping," which can greatly reduce thermal conductivity. Maznev [27] investigated elastic wave scattering from a nearly smooth surface using a Green's function technique and found that most energy from a normally incident longitudinal wave can undergo mode conversion into Rayleigh waves.

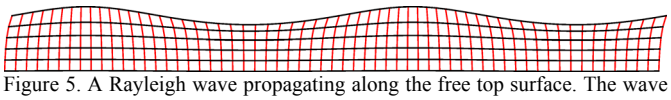

Figure 5. A Rayleigh wave propagating along the free top surface. The wave amplitude decays exponentially with increasing distance from the surface. Reprinted with permission from Ref. [32], copyright APS 2016.

Elastic materials are a simpler, long-wavelength limit of atomic materials and they support acoustic longitudinal, acoustic transverse, Rayleigh, and structure-dependent modes (such as torsional modes for a wire). The study of elastic continuum materials can provide important insights into phonon-surface scattering in atomic materials, especially for long-wavelength modes in the nanostructures that are too large to treat directly using atomistic techniques, yet too small to be considered bulk. We developed an efficient finite-difference time-domain (FDTD) solution to the elastic and scalar wave equations and coupled it with the Green-Kubo formula to calculate thermal conductivity in the elastic solid approximation [32]. The combination of FDTD and Green-Kubo has similarities to an equilibrium molecular dynamics (MD) simulation, but scales better than MD as the system size increases and enables us to simulate large nanostructures with pronounced roughness. We simulated two-dimensional (2D) graphenelike nanoribbons with random, rough edges using both elastic and scalar waves with free and fixed boundary conditions (BCs). These combinations of wave equations and BCs let us selectively "turn off" Rayleigh waves and mode conversion to study their effects: scalar waves, which are the basis for the concept of the specularity parameter, do not support mode conversion at all. Elastic waves support bulk mode conversion at the surface, but only elastic waves with free boundary conditions (e.g., in suspended nanostructures) allow for Rayleigh waves.

We find that mode conversion between bulk modes has a minor effect on heat conduction; in fact, the effect of bulk-to-bulk mode conversion can effectively be subsumed in the

partially diffuse scattering model. In the phonon language, mode conversion results in some probability of a phonon scattering into a different bulk mode with same energy, and with the modal outgoing waves at very specific angles with respect to surface normal; however, since the surface is rough, the result is overall equivalent to partially diffuse scattering (Fig. 6). In contrast, mode conversion between bulk and Rayleigh waves can drastically reduce thermal conductivity because it amounts to energy trapping. In the phonon language, mode conversion from bulk to Rayleigh waves means that the phonon has a finite probability to become akin to absorbed – its energy becomes trapped at the surface in the Rayleigh mode that is either very slow or easily confined by roughness (Fig. 6).

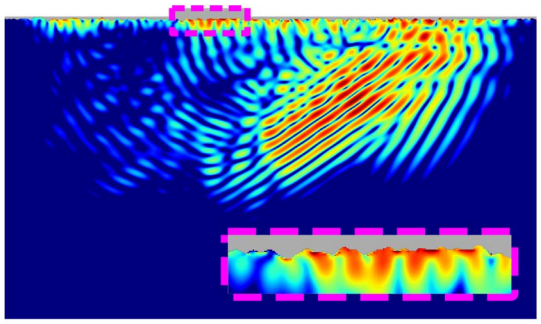

Figure 6. Snapshots of an elastic wave scattered wave from a rough free surface at the top; the incoming wave was longitudinal. Color represents the energy-density profile (log scale, arbitrary units; red: high, blue: low). In the scattered wave profile, Rayleigh modes are visible (energy is localized near the free surfaces); such modes do not exist for fixed surfaces. (Inset) Zoom-in on the energy-density profile inside the dashed box on the main panel reveals a localized Rayleigh surface mode. Reprinted with permission from Ref. [32], copyright APS 2016.

III. Interfaces: Thermal Transport In Heterostructures and Superlattices

Layered heterostructures are a common building block of state-of-the-art electronic and optoelectronic devices. The interfaces are atomically rough [4,5], which somewhat degrades electronic transport, but other benefits, such as design flexibility, justify this approach. However, interfacial roughness and the large mismatch between the vibrational densities of states in neighboring layers are greatly disruptive to phonon transport [1,2].

Thermal boundary resistance (TBR) exists at interfaces because of the non-unity phonon transmission rate. When a temperature difference is applied to the two sides of the interface, there will be an abrupt temperature drop [33]. The TBR is defined as $R=\Delta T/J_Q$, where J_Q is the heat flow perpendicular to the interface and ΔT is the temperature difference between the two sides of the interface. The drop indicates that TBR is comparable to or even greater than the layer thermal resistance in the cross-plane direction. At a heterointerface, TBR would exist due to acoustic mismatch, even if the interface were atomically perfect. In superlattices (SLs), multiple interfaces between different materials play a critical role in thermal transport. Experiments on cross-plane thermal conductivity of superlattices (SLs) show that the existence of TBR dominates the cross-plane thermal transport [34-39]. On the other hand, since TBR is mainly related to the transmission of phonons from one material to another. Phonon transport parallel to the interface (in-plane) is affected less, and mostly through interface roughness; the effect is discussed in detail in Ref. [40]. Therefore, thermal transport in the presence of interfaces is very anisotropic, especially when there are multiple interfaces present, as in SLs [1,2].

The ability to accurately describe thermal transport across interfaces is extremely valuable in the thermal analysis of devices, yet modeling of interfacial heat transport remains a challenge. The acoustic mismatch model (AMM) [41] and the diffuse mismatch model (DMM) [42] are two key approaches: AMM calculates the transmission rate following Snell's law, while DMM calculates the transmission rate as if the interface were completely momentum randomizing. Neither model can accurately capture the phonon transport behavior at realistic, high-quality interfaces, where transmission is a combination of specular and diffuse.

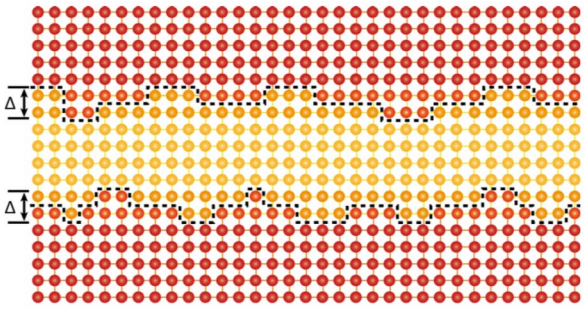

Figure 7. The interfaces in superlattices are of extremely high quality, but atomic scale roughness strongly affects thermal transport and leads to anisotropy in heat conduction. Reprinted with permission from Ref. [40], copyright AIP 2015.

Phenomenological models cannot capture the actual morphology of the interface, including interfacial atom mixing. Therefore, molecular dynamics (MD) simulations, where classical motion of atoms is explicitly followed in space, have an advantage. Both equilibrium MD (EMD) [43] and nonequilibrium MD (NEMD) [44] techniques can be used to obtain TBRs. MD is capable of modeling any interface, whether it is solid-liquid [45], smooth solid-solid [44], or solid-solid with interfacial atom mixings [46]. However, the quality of the obtained TBR hinges on the choice of the empirical potentials used to describe atom motion. Further, MD often suffers from the size effect of the simulation cell, which has to be countered [47]. Nonequilibrium Green's functions method is another atomistic method that can capture the atomic-level detail at the interface. However, its application to interfacial transport has been limited by computational burden [48,49]. A recent FDTD study [32] shows that, apart from introducing TBR and making thermal transport anisotropic, rough interfaces cause propagating phonon modes to convert to Rayleigh modes and become more localized. The localization of phonon modes not only further decreases thermal conductivity, but also creates hot spots at the rough areas of the interface, which harms both the performance and the reliability of the devices.

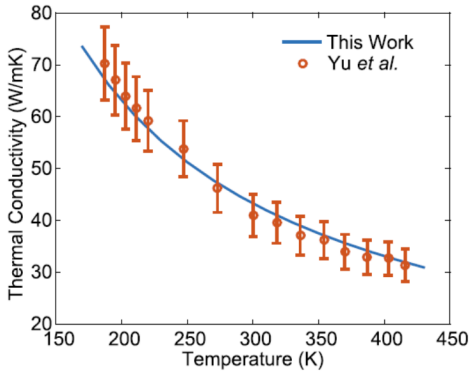

Figure 8. In-plane thermal conductivity of a GaAs/AlAs superlattice (layer thickness 70 nm) as a function of temperature. Red symbols show the experimental results of Yu *et al.* [59], and the blue curve shows the calculations from our model. Reprinted with permission from Ref. [40], copyright AIP 2015.

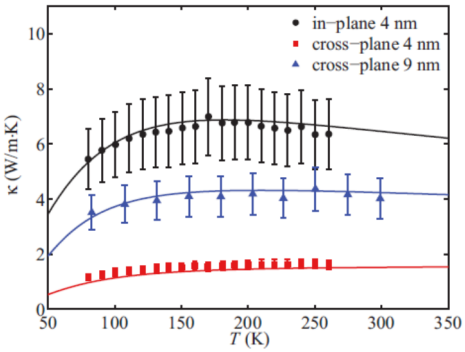

Figure 9. Thermal conductivity of a 9-nm-period Si/Ge superlattice in the cross-plane direction [(blue) triangles] and a 4-nm-period Si/Ge superlattice in both the in-plane [(black) circles] and the cross-plane directions [(red) squares]. Experimental data are represented by symbols. The anisotropy between the in-plane and the cross-plane directions, as well as the thickness and temperature dependence, is well explained by our momentum-dependent interface roughness scattering model. Reprinted with permission from Ref. [60], copyright APS 2013.

We present a semiclassical model describing the full thermal conductivity tensor of III-V compound SL structures and apply it to III-arsenide systems (Fig. 8). The phonon transport inside each layer is captured by solving the phonon Boltzmann transport equation (PBTE) in the relaxation-time approximation (RTA), with rates describing the common internal scattering mechanisms as well as the partially diffuse scattering from the interfaces. The in-plane thermal conductivity is obtained from the layers connected in parallel, while the cross-plane conductivity is calculated from the layers and TBRs in series. The TBR of each interface is calculated by interpolating between the AMM and DMM transmission coefficients. Both the partially diffuse interface scattering and the AMM-DMM interpolation are described with the aid of the same momentum-dependent specularity parameter, in which there is a single adjustable parameter—an effective interface rms roughness. The model can effectively describe complicated systems with an arbitrary number of interfaces and random layer thicknesses. Despite the model simplicity, the calculation results agree well with experimental data from multiple studies by different groups. The model is also quite general: it is applicable to SLs in other material systems with good-quality interfaces and semiclassical phonon transport (Fig. 9).

IV. Point Defects and Mass Difference Scattering: Thermal Transport in Alloys

Doping and alloying are commonly used to tune the electronic properties of semiconductor nanostructures. Both effectively introduce point defects in the crystalline matrix and are mainly detrimental to phonon transport. Since both doping and alloying introduce alien atoms to the original crystal, they introduce extra mass-difference scattering for phonons. Additionally, for alloys, especially the ones where two materials are almost equally mixed, phonon dispersions can deviate a lot from those of the single crystals. With very high doping or near-equal-parts alloying, thermal conductivity becomes much lower than in single crystals (Fig. 10). Alloying promotes anisotropy and can lead to a qualitatively new "superdiffusive" phonon transport regime [50].

Experiments show that phonon interaction with dopants affects the thermal conductivity more at lower temperatures and becomes less important at higher temperatures [51]. Alloying, on the other hand, can reduce thermal conductivity by an order of magnitude [51]. The authors of [51], [52], and [53] measured thermal conductivity of GaAsP, InGaAs, and GaAlAs alloys; the equal-parts alloy thermal conductivity is only ~20% of the bulk thermal conductivities.

Abeles [54] first proposed the virtual crystal approximation (VCA) and applied the Klemens–Callaway model for the mass-difference scattering rate. In Ref. [40], this scattering rate is adopted to accurately describe the thermal conductivity of doped GaAs and InGaAs and GaAlAs ternary alloys with various doping levels and compositions. In ternary alloys, the adiabatic bond-charge model (ABCM) [55–57] is used to calculate the full phonon dispersion for each alloy composition. Khatami and Aksamija [58] used a similar model on group IV alloys and found a broad plateau for alloy concentrations between 0.2 and 0.8 in alloys (Fig. 10). Further, temperature dependence of the thermal conductivity is also largely suppressed. However, the validity of the VCA is limited to the cases when the mass difference is relatively small; otherwise, atomistic approaches are necessary [61].

Alloy scattering is the dominant mechanism that influences the thermal conductivity of ternary compounds. Unfortunately, very few experiments (see an overview in Ref. [40]) have been carried out on III-As compounds and they were all performed at room temperature. In Figures 11 and 12, we compare our calculated thermal conductivity of $In_xGa_{1-x}As$ and $Al_xGa_{1-x}As$ with various compositions with experimental results. Our calculations agree well with the available experimental data over a wide range of compositions (Figs. 11 and 12). To our knowledge, no systematic measurements of the thermal conductivity of $In_xAl_{1-x}As$ have been carried out thus far.

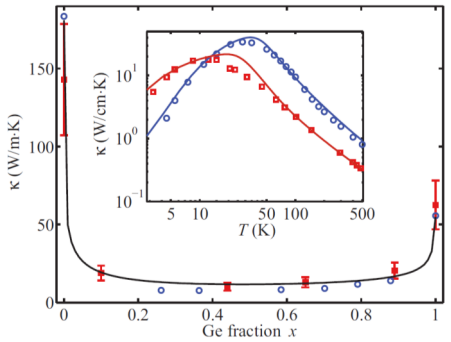

Figure 10. Thermal conductivity of bulk $Si_{1-x}Ge_x$, showing a strong dependence on the germanium fraction x. The thermal conductivity of bulk alloys quickly decreases with increasing x, then reaches a plateau for $0.2 < x < 0.8$. Experimental data points are shown for comparison, demonstrating excellent agreement with the model. Inset: The calculated thermal conductivity shows excellent agreement with the measurements on for bulk Si [(blue) circles] and Ge [(red) squares] over a wide range of temperatures. Reprinted with permission from Ref. [60], copyright APS 2013.

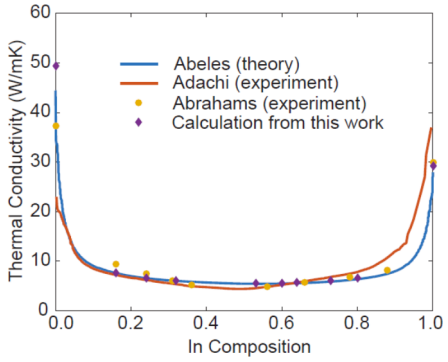

Figure 11. Thermal conductivity of bulk $In_xGa_{1-x}As$ with varying In composition. The blue curve shows the theoretical results from Abeles [54]. The red curve and orange dots present the experimental results from Adachi [52] and Abrahams *et al.* [62] respectively. Purple diamonds represent the results of our calculation.

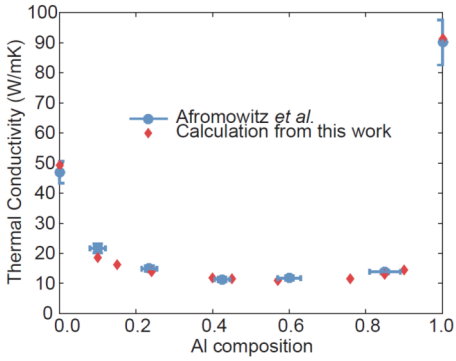

Figure 12. Thermal conductivity of bulk $Al_xGa_{1-x}As$ with varying Al composition. Blue dots and red diamonds show the experimental data of Afromowitz *et al*. [53] and the results of calculation in [40].

V. Strain: Thermal Transport In Strained Thin Films

Strain is common in heterostructures and superlattices, as the layers of different bulk lattice constants are grown side by side. As a crystal lattice is stretched (compressed) along the growth direction, it is compressed (stretched) along another; therefore, straining leads to crystalline anisotropy. With strain, the electron band structure and phonon dispersions also change. Strain is sometimes intentionally introduced into electronic systems to achieve enhanced electron/hole mobility.

Direct measurements on thermal transport with strain are difficult, because it is impossible to fabricate strained bulk materials. Thermal conductivity of strain-balanced SLs (alternating layers have balancing tensile and compressive strain with the overall structure being strain-free) can be measured directly, but a careful analysis is needed to extract the effect of strain alone. From previous indirect measurements in QCL devices, the thermal conductivity of a strain-balanced SL decreases with increasing strain in each layer [63–66]. The decreased thermal conductivity results in slower heat extraction and greater local heating, which eventually causes the device to break down.

The strain effect on thermal transport can be treated through an effective scattering rate within the PBTE and relaxation-time approximation [67]. Like the mass-difference scattering, as strain increases, the applicability of this perturbation model decreases. Recently, Foss and Aksamija [68] extended the use of this model and applied it to strained Si and Ge thin films. In order to fully capture the effects of strain, the authors calculated the phonon dispersion of Si and Ge under compressive and tensile biaxial strains using first-principles density functional perturbation theory (DFPT). All simulations were performed with the open-source software Quantum-ESPRESSO [69] (www.quantum-espresso.org). Biaxial strain was applied by fixing the lattice constant in the *xy*-plane and allowing the out-of-plane (*z*-axis) lattice constant to relax energetically.

The in-plane (IP) and cross-plane (CP) thermal conductivities (κ_{IP} and κ_{CP}) of finite-volume thin films of strained silicon and germanium were calculated from 0 to 500 K (Fig. 13). A surface rms roughness height of 0.45 nm is used as a typical value in calculating the boundary scattering with roughened surfaces. The corresponding IP and CP lattice directions are [100] and [001], respectively. The thermal conductivities are presented in Fig. 13, where the in-plane conductivity is in good agreement with previous theoretical (based on the PBTE and the relaxation-time approximation) and experimental studies on silicon-on-insulator samples. We note that, similar to our previous studies on silicon, an anisotropy factor (κ_{IP}/κ_{CP}) of 2 is observed at room temperature due to boundary scattering. In thin Ge films, an anisotropy factor of 1.8 is found.

The strain dependence for semiconductor nanostructures is moderate for both Si and Ge. However, for κ_{CP} at temperatures above roughly 100 K, compressive (tensile) strain can be seen to strongly increase (reduce) the overall conductivity. To better illustrate the strain dependence, the bottom panels in Fig. 13 show the percent change in $\kappa_{IP,CP}$ as a function of applied strain at room temperature. We see a clear decreasing trend from a maximum boost of ~20% in Si (~25% in Ge) at 4% compressive strain to a decrease of ~15% in Si (~16% in Ge) in the CP conductivity at 4% tensile strain, while the IP conductivity remains relatively unchanged with

variations <5% in Si (<10% in Ge) compared to the unstrained material. The IP conductivity is driven by phonons with large IP components of the group velocity; they interact less with boundary roughness, which is dependent on the CP velocity. Tensile strain reduces the heat capacity and IP velocity, but also the CP velocity, thereby resulting in less boundary scattering, and the two trends cancel out.

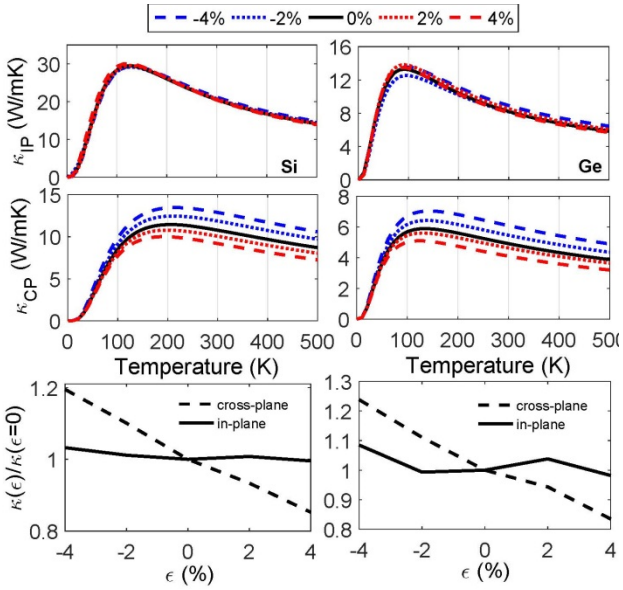

Figure 13. The in-plane (top) and cross-plane (middle) thermal conductivities for 20-nm-thick silicon (left) and germanium (right) thin films with 0.45-nm surface roughness from 0 to 500 K. Strained materials are represented by blue (compressive) and red (tensile) dotted and dashed lines. (bottom) Change in thermal conductivity relative to the unstrained case as a function of strain for a 20-nm-thin film with surface roughness 0.45 nm at 300 K, showing significant strain dependence of cross-plane conductivity. Reprinted with permission from Ref. [68], copyright AIP 2016.

In contrast, CP transport depends only on the CP component of phonon velocity, so phonons having a higher CP velocity (directed into the boundary) contribute more to CP transport, but they also encounter more boundary scattering. Hence, as tensile strain reduces both the CP velocity and heat capacity, the two trends add up and result in a much more pronounced strain modulation than observed in the IP conductivity. In addition, strain inherently promotes anisotropic transport by breaking lattice symmetry between the direction(s) of the applied strain and the direction(s) perpendicular to the applied strain direction. Our results indicate that heat removal from strained thin-film devices can be improved by compressive strain, because compressive strain increases the CP heat flow up to 20%. We conclude that strain engineering can be an effective way to modulate the thermal conductivity in Si and Ge nanostructures in the direction perpendicular to their boundaries.

VI. A Device Example: The Quantum Cascade Laser

Superlattices based on III-V compound semiconductors have widespread use in optoelectronics. In quantum cascade lasers (QCLs), self-heating is the main issue limiting the development of room-temperature, continuous-wave lasing, which is exacerbated by the poor thermal conduction through hundreds of interfaces in a typical structure. A good understanding of the influence of interfaces on the thermal conductivity tensor of III-V SLs would enable advances in the design and modeling and optoelectronic devices for enhanced reliability.

The quantum cascade laser (QCLs) is a unique system to study the effects of thermal stress on electronic devices because it brings all the previously discussed disorders together. The active core of a QCL is a III-V SL, consisting of hundreds of layers and therefore many interfaces. To engineer the bandstructure and ultimately the lasing wavelength, these III-V SLs often incorporate ternary alloys, which brings about mass-difference scattering. Some layers inside the active core are also doped, which leads to more mass-difference scattering. Since the whole device is built on GaAs or InP substrates, the layer thicknesses are carefully designed so that the SL is strain-balanced, while individual layers are tensilely or compressively strained. Furthermore, QCL is also a system where electronic transport and thermal transport are closely coupled [70]. The interfaces, point defects, and the strain affect both the electronic and phononic system, which also exchange energy with each other. Both electrons and phonons are far from equilibrium ("hot") [70].

Today, room-temperature , continuous-wave lasing in the mid-infrared (mid-IR) spectrum has been demonstrated in InGaAs(wells)/ InAlAs(barriers) systems on an InP substrate [71-74,64,65]. Applications of these lasers in sensing and communication require long-term-reliable QCLs lasing between 3 – 5 μm with high optical power. The long-term reliability hinges on the long-term structural integrity of the core, including the facets, under the extreme thermal stress caused by interfaces, point defects, and strain. To analyze and design such devices, it is important to thoroughly study the coupled electrothermal nonequilibrium transport inside the QCL system [70,75].

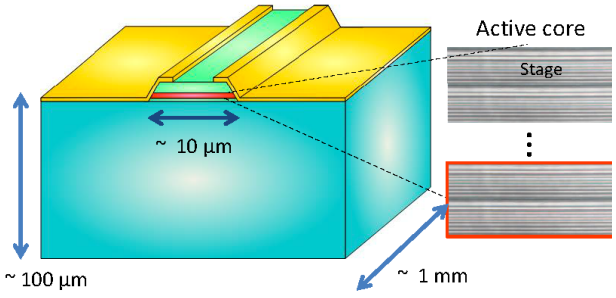

Figure 14. The multiscale nature of the QCL transport problem. While electron transport and optical-field emission occur in the active core of the device and can be electrically controlled, thermal transport involves the entire large device and is only controlled via thermal boundary conditions that can be far from the active core.

Figure 14 is a schematic of a typical QCL device. The active core consists of hundreds of layers, and is ~1 μm thick and ~10 μm wide. The active core is sandwiched between

roughly 5-µm-thick cladding layers and placed on top of a substrate that is ~100 µm thick and ~1 mm wide. The bottom of the substrate often sits on a heat reservoir and the rest of the boundaries have convective (single device) or adiabatic (laser array) boundary conditions. Interesting electronic transport and optical-field emission happen only inside the active core, meaning the main heat generation processes are inside the active core. While electronic transport is mainly confined, the generated heat must travel through the whole device to reach the boundary and get extracted—the thermal transport is controlled via thermal boundary conditions that exist far away from the active core. Therefore, the coupled electrothermal transport is a multi-scale problem.

The materials in the active core have low thermal conductivities, as they are alloys and sometimes doped. The presence of multiple interfaces and strain further reduces thermal conductivity and additionally makes the thermal transport very anisotropic—cross-plane thermal conductivity is severely suppressed while in-plane thermal conductivity is less affected (Fig. 15). The active core is significantly hotter than the rest of the device, being that it acts as the main heat source and has poor and very anisotropic heat conduction. Moreover, the existence of interfacial roughness may trap heat at the interfaces [32], further reduce thermal conductivity, and increase the heating in the active core.

Figure 16 shows a typical temperature profile of the cross-section of a GaAs/GaAlAs-based QCL lasing at 9 µm [75] from our simulation. Here, the bottom of the device is connected to a heat sink at 77 K while the other boundaries are in an adiabatic environment. The current density across the active core is 6 kA/cm^2 in this case. We see that the active core has a much higher temperature than the rest of the structure. The temperature difference and the low core thermal conductivity together create a high temperature gradient at the interfaces and the facets. With prolonged operation, the thermal stress will expedite the degradation of the interfaces and the facets and eventually threaten the long-term reliability of the device [77].

The presence of interfaces affects the device reliability through more ways than simply reducing thermal conductivity. Scattering of electrons due to interface-roughness (IR) is the main gain broadening mechanism in mid-IR QCLs, which reduces optical gain. This effect is illustrated in Fig. 17, which shows the calculated gain spectrum for the 4.6-micron QCL proposed in [72]. The results are shown with and without the inclusion of interface-roughness scattering.

The reduced peak gain means that in order to achieve lasing, higher electric fields and currents density are involved, causing more heating and reduced device lifetime. As an example, Fig. 18(a) shows the simulated current density vs field strength for the same 4.5 micron QCL, with and without the inclusion of interface-roughness scattering. In Fig. 18(a), we can see that the presence of IR scattering has minimal effects on the simulated current density. However, in Fig. 18(b), we see that with IR scattering included, the peak gain is drastically lower for all field values. With IR scattering included, the predicted threshold current density is

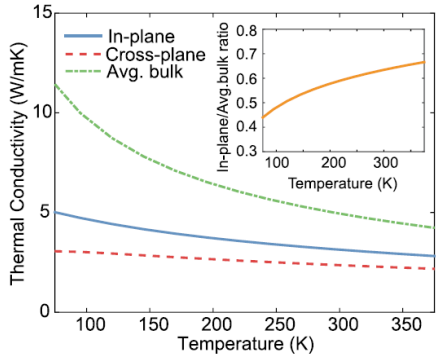

Figure 15. Thermal conductivity of a typical QCL active region65 as a function of temperature. A single stage consists of 16 alternating layers of $In_{0.53}Ga_{0.47}As$ and $In_{0.52}Al_{0.48}As$. Blue solid curve, red dashed curve, and green dashed-dotted curve are showing the calculated in-plane, cross-plane, and the averaged bulk thermal conductivity, respectively. Δ=1 Å in the calculations The inset shows the ratio between the calculated in-plane and the averaged bulk thermal conductivities. Reprinted with permission from Ref. [40], copyright AIP 2015.

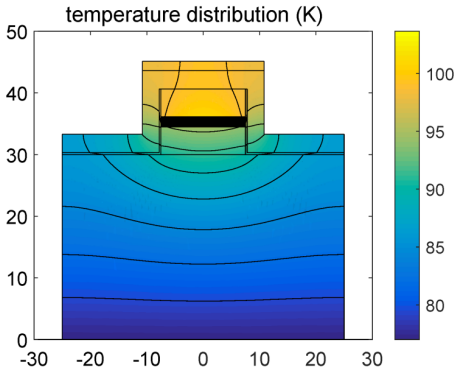

Figure 16. A typical temperature profile of the cross-section of a GaAs/GaAlAs-based QCL device. The bottom of the device is connected to a heat sink held at 77 K and adiabatic boundary conditions are applied elsewhere. The current density across the active core is 6 kA/cm^2. The temperature at the active core is significantly higher than the rest of the device and the temperature gradient is largest at interfaces and facets.

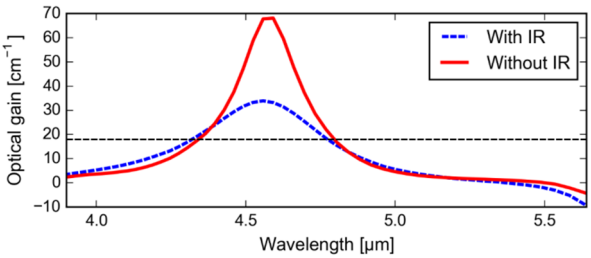

Figure 17. Calculated gain spectrum for the 4.6-micron QCL proposed in [2]. Results are shown for the maximum operating field of 75 kV/cm. Dashed horizontal line represents the estimated threshold gain of 18 cm^{-1}. The data is obtained using a density-matrix model proposed in Ref. [77].

1.67 kA/cm^2 at the experimentally determined threshold field of 64 kV/cm, which corresponds to a threshold gain of approximately 18 cm^{-1}. However, if IR scattering is turned off, the threshold gain is obtained at a much lower current density of 0.95 kA/cm^2 and electric field of 60 kV/cm. The lower current and field represents a lowering of Joule heating (product of current density and electric field) by a factor of

1.9, which represent a drastic reduction in input power. Of course interface roughness can never be completely eliminated. However, these results indicate how reliability can be greatly increased by minimizing interface roughness during the growth process.

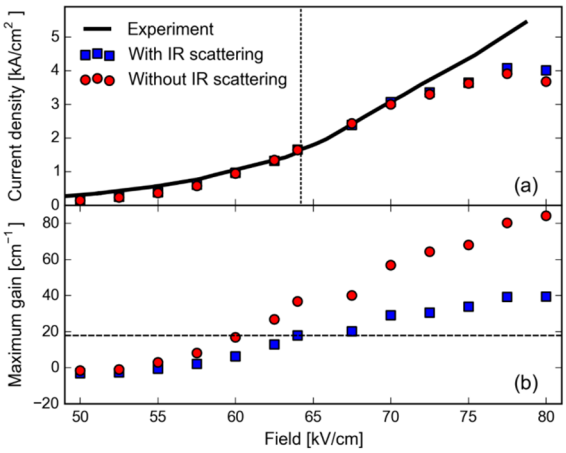

Figure 18. (a) Current density vs applied field at room temperature for the 4.6-μm QCL proposed in Ref. [2]. The solid line shows experimental results and blue (red) squares (circles) show theoretical results with (without) interface roughness scattering included. The dashed vertical line represents the measured threshold field of 64 kV/cm. (b) Calculated peak gain as a function of electric field with interface roughness included (blue squares) and not included (red circles). Dashed horizontal line represents the estimated threshold gain of 18 cm^{-1}. All theoretical results are obtained using a density-matrix model proposed in Ref. [78].

VII. Conclusion

In summary, we discussed how boundaries, interfaces, mass-difference scattering, and strain affect thermal transport in modern semiconductor nanostructures and devices. These different types of disorder stem from the use of common fabrication techniques that are usually meant to improve the desired electronic or optical performance. Therefore, it is critical to understand the accompanying detrimental effects, such as anisotropic thermal conduction and localized heating, which have a significant adverse effect on device operation and long-term reliability, and should be a critical design consideration.

References

[1] D. G. Cahill, W. K. Ford, K. E. Goodson, G. D. Mahan, A. Majumdar, H. J. Maris, R. Merlin, and S. R. Phillpot, "Nanoscale thermal transport," *J. Appl. Phys.* 93, 793, 2003.

[2] D. G. Cahill, P. V. Braun, G. Chen, D. R. Clarke, S. Fan, K. E. Goodson, P. Keblinski, W. P. King, G. D. Mahan, A. Majumdar, H. J. Maris, S. R. Phillpot, E. Pop, and L. Shi, "Nanoscale thermal transport. II. 2003–2012," *Appl. Phys. Rev.* 1, 011305, 2014.

[3] G. P. Srivastava, *The Physics of Phonons*, New York: Taylor & Francis, 1990.

[4] K. Cheng, "Molecular beam epitaxy technology of III-V compound semiconductors for optoelectronic applications," *Proc. IEEE* **85**, 1694, 1997.

[5] K. Goetz, D. Bimberg, H. Jüurgensen, J. Selders, A. V. Solomonov, G. F. Glinskii, and M. Razeghi, "Optical and crystallographic properties and impurity incorporation of $Ga_xIn_{1-x}As$ ($0.44<x<0.49$) grown by liquid phase epitaxy, vapor phase epitaxy, and metal organic chemical vapor deposition," *J. Appl. Phys.* 54, 4543, 1983.

[6] E. Pop, S. Sinha, and K. Goodson, "Heat generation and transport in nanometer-scale transistors," *Proc. IEEE* 94, 1587, 2006.

[7] K. Raleva, D. Vasileska, S. M. Goodnick, and M. Nedjalkov, "Modeling thermal effects in nanodevices," *IEEE Trans. Electron Devices* 55, 1306, 2008.

[8] E. Pop, "Energy dissipation and transport in nanoscale devices," *Nano Res.* 3, 147, 2010.

[9] J. Towns *et al.,* "XSEDE: Accelerating Scientific Discovery," *Comput. Sci. Eng.* 16, 62–74 (2014).

[10] Akram I. Boukai, Yuri Bunimovich, Jamil Tahir-Kheli, Jen-Kan Yu, William A. Goddard III, & James R. Heath, "Silicon nanowires as efficient thermoelectric materials," *Nature* 451, 168-171, 2008.

[11] A. I. Hochbaum, Renkun Chen, Raul Diaz Delgado, Wenjie Liang, Erik C. Garnett, Mark Najarian, Arun Majumdar, & Peidong Yang, "Enhanced thermoelectric performance of rough silicon nanowires," *Nature* 451, 163-167, 2008.

[12] Joseph P. Feser, Jyothi S. Sadhu, Bruno P. Azeredo, Keng H. Hsu, Jun Ma, Junhwan Kim, Myunghoon Seong, Nicholas X. Fang, Xiuling Li, Placid M. Ferreira, Sanjiv Sinha, and David G. Cahill, "Thermal conductivity of silicon nanowire arrays with controlled roughness," *J. Appl. Phys.* 112, 114306, 2012.

[13] J. Lim, K. Hippalgaonkar, S. C. Andrews, A. Majumdar, and P. Yang, "Quantifying surface roughness effects on phonon transport in silicon nanowires," *Nano Lett.* 12, 2475, 2012.

[14] J. Ziman, *Electrons and Phonons: The Theory of Transport Phenomena in Solids*, New York: Oxford University Press, 1960.

[15] Yunfei Chen, Deyu Li, Jennifer R. Lukes and Arun Majumdar, "Monte Carlo Simulation of Silicon Nanowire Thermal Conductivity," *J. Heat Transfer* 127, 1129-1137, 2005.

[16] M.-H. Bae, Z. Li, Z. Aksamija, P. N. Martin, F. Xiong, Z.-Y. Ong, I. Knezevic, and E. Pop, "Ballistic to diffusive crossover of heat flow in graphene ribbons," *Nature Communications* 4, 1734, 2013.

[17] S. Mei, L. N. Maurer, Z. Aksamija, and I. Knezevic, "Full-dispersion Monte Carlo simulation of phonon transport in micron-sized graphene nanoribbons," *J. Appl. Phys.* 116, 164307, 2014.

[18] Z. Aksamija and I. Knezevic, "Anisotropy and boundary scattering in the lattice thermal conductivity of silicon nanomembranes," *Physical Review B* 82, 045319, 2010.

[19] Z. Aksamija and I. Knezevic, "Lattice thermal conductivity in $Si_{1-x}Ge_x/Si_{1-y}Ge_y$ superlattices: Competition between interfacial and internal scattering," *Physical Review B* 88, 155318, 2013.

[20] D. A. Broido, M. Malorny, G. Birner, N. Mingo, and D. A. Stewart, "Intrinsic lattice thermal conductivity of semiconductors from first principles," *Appl. Phys. Lett.* 91, 231922, 2007.

[21] L. N. Maurer, Z. Aksamija, E. B. Ramayya, A. H. Davoody, and I. Knezevic, "Universal features of phonon transport in nanowires with correlated surface roughness," *Appl. Phys. Lett.* 106, 133108, 2015.

[22] A.H. Davoody, E. B. Ramayya, L. N. Maurer, and I. Knezevic, "Ultrathin GaN Nanowires: Electronic, Thermal, and Thermoelectric Properties," *Physical Review B* 89, 115313, 2014.

[23] E. B. Ramayya, L. N. Maurer, A. H. Davoody, and I. Knezevic, "Thermoelectric properties of ultrathin silicon nanowires," *Physical Review B* 86, 115328, 2012.

[24] Yuping He and Giulia Galli, "Microscopic Origin of the Reduced Thermal Conductivity of Silicon Nanowires," *Phys. Rev. Lett.* 108, 215901, 2012.

[25] R. F. Wallis, "Lattice dynamics of crystal surfaces," *Prog. Surf. Sci.* 4, 233-367, 1974.

[26] R. F. Wallis, "Surface phonons: theoretical developments," *Surf. Sci.* 299-300, 612-627, 1994.

[27] A.A. Maznev, "Boundary scattering of phonons: Specularity of a randomly rough surface in the small-perturbation limit," *Phys. Rev. B* 91, 134306, 2015.

[28] L.D. Landau and E.M. Lifshitz, *Theory of Elasticity*, Pergamon Press, 1986.

[29] B. Garber, M. Cahay, and G. E. W. Bauer, "Localization of Rayleigh waves," *Phys. Rev. B* 62, 12831-12837, 2000.

[30] T. Nakayama, "Diffuse scattering of high-frequency phonons at solid

surfaces," *Phys. Rev. B* 32, 777-780, 1985.

[31] By. Kang and S. K. Estreicher, "Thermal conductivity of Si nanowires: A first-principles analysis of the role of defects," *Phys. Rev. B* 89, 155409, 2014.

[32] L. N. Maurer, S. Mei, and I. Knezevic, "Rayleigh waves, surface disorder, and phonon localization in nanostructures," *Phys. Rev. B* 94, 045312, 2016.

[33] G. Chen, "Thermal conductivity and ballistic-phonon transport in the cross-plane direction of superlattices," *Phys. Rev. B* 57, 14958, 1998.

[34] G. Chen, C. L. Tien, X. Wu, and J. S. Smith, "Thermal diffusivity measurement of GaAs/AlGaAs thin-film structures," *J. Heat Transfer* 116, 325, 1994.

[35] W. Capinski and H. Maris, "Thermal conductivity of GaAs/AlAs superlattices," *Physica B* 219–220, 699, 1996.

[36] S.-M. Lee, D. G. Cahill, and R. Venkatasubramanian, "Thermal conductivity of Si–Ge superlattices," *Appl. Phys. Lett.* 70, 2957, 1997.

[37] W. S. Capinski, H. J. Maris, T. Ruf, M. Cardona, K. Ploog, and D. S. Katzer, "Thermal-conductivity measurements of GaAs/AlAs superlattices using a picosecond optical pump-and-probe technique," *Phys. Rev. B* 59, 8105, 1999.

[38] S. T. Huxtable, A. R. Abramson, C.-L. Tien, A. Majumdar, C. LaBounty, X. Fan, G. Zeng, J. E. Bowers, A. Shakouri, and E. T. Croke, "Thermal conductivity of Si/SiGe and SiGe/SiGe superlattices," *Appl. Phys. Lett.* 80, 1737, 2002.

[39] A. Sood, J. A. Rowlette, C. G. Caneau, E. Bozorg-Grayeli, M. Asheghi, and K. E. Goodson, "Thermal conduction in lattice–matched superlattices of InGaAs/InAlAs," *Appl. Phys. Lett.* 105, 051909, 2014.

[40] S. Mei and I. Knezevic, "Thermal conductivity of III-V semiconductor superlattices," *J. Appl. Phys.* 118(17), 175101, 2015.

[41] I. M. Khalatnikov, *Zh. Eksp. Teor. Fiz.* 22, 687, 1952.

[42] E. T. Swartz and R. O. Pohl, "Thermal boundary resistance," *Rev. Mod. Phys.* 61, 605, 1989.

[43] Y. Chalopin, K. Esfarjani, A. Henry, S. Volz, and G. Chen, "Thermal interface conductance in Si/Ge superlattices by equilibrium molecular dynamics," *Phys. Rev. B* 85, 195302, 2012.

[44] E. S. Landry and A. J. H. McGaughey, "Thermal boundary resistance predictions from molecular dynamics simulations and theoretical calculations," *Phys. Rev B* 80, 165304, 2009.

[45] S. Maruyama and T. Kimura, "Molecular Scale Aspects of Liquid Contact on a Solid Surface," *Therm. Sci. Eng.* 7(1), pp. 63-68, 1999.

[46] S. C. Huberman, J. M. Larkin, A. J. H. McGaughey, and C. H. Amon, "Disruption of superlattice phonons by interfacial mixing," *Phys. Rev. B* 88, 155311, 2013.

[47] Z. Liang and P. Keblinski, "Finite-size effects on molecular dynamics interfacial thermal-resistance predictions," *Phys. Rev. B* 90, 075411, 2014.

[48] N. Mingo and L. Yang, "Phonon transport in nanowires coated with an amorphous material: An atomistic Green's function approach," *Phys. Rev. B* 68, 245406, 2003.

[49] P. E. Hopkins, P. M. Norris, M. S. Tsegaye, and A. W. Ghosh, "Extracting phonon thermal conductance across atomic junctions: Nonequilibrium Green's function approach compared to semiclassical methods," *J. Appl. Phys.* 106, 063503, 2009.

[50] M. Upadhyaya and Z. Aksamija, "Nondiffusive lattice thermal transport in Si-Ge alloy nanowires," *Phys. Rev. B* 94, 174303, 2016.

[51] R. O. Carlson, G. A. Slack, and S. J. Silverman, "Thermal conductivity of GaAs and GaAs1−xPx laser semiconductors," *J. Appl. Phys.* 36(2), pp. 505-507, 1964.

[52] S. Adachi, "Lattice thermal resistivity of III–V compound alloys," *J. Appl. Phys.* 54, 1844, 1983.

[53] M. A. Afromowitz, "Thermal conductivity of $Ga_{1-x}Al_xAs$ alloys," *J. Appl. Phys.* 44, 1292, 1973.

[54] B. Abeles, "Lattice thermal conductivity of disordered semiconductor alloys at high temperatures," *Phys. Rev.* 131, 1906, 1963.

[55] W. Weber, "New bond-charge model for the lattice dynamics of diamond-type semiconductors," *Phys. Rev. Lett.* 33, 371, 1974.

[56] K. Rustagi and W. Weber, "Adiabatic bond charge model for the phonons in A^3B^5 semiconductors," *Solid State Commun.* 18, 673, 1976.

[57] H. M. Tütüncü and G. P. Srivastava, "Phonons in zinc-blende and wurtzite phases of GaN, AlN, and BN with the adiabatic bond-charge model," *Phys. Rev. B* 62, 5028, 2000.

[58] S. N. Khatami and Z. Aksamija, "Lattice thermal conductivity of the binary and ternary group-IV alloys Si-Sn, Ge-Sn, and Si-Ge-Sn," *Phys. Rev. Appl.* 6, 014015, 2016.

[59] X. Y. Yu, G. Chen, A. Verma, and J. S. Smith, "Temperature dependence of thermophysical properties of GaAs/AlAs periodic structure," *Appl. Phys. Lett.* 67, 3554, 1995.

[60] Z. Aksamija and I. Knezevic, "Lattice thermal conductivity in $Si_{1-x}Ge_x/Si_{1-y}Ge_y$ superlattices: Competition between interfacial and internal scattering," *Phys. Rev. B* 88, 155318, 2013.

[61] T. Shiga, T. Hori, and J. Shiomi, "Influence of mass contrast in alloy phonon scattering," *Jpn. J. Appl. Phys.* 53, 021802, 2014.

[62] M. Abrahams, R. Braunstein, and F. Rosi, "Thermal, electrical and optical properties of (In,Ga)As alloys," *J. Phys. Chem. Solids* 10, 1959.

[63] H. K. Lee and J. S. Yu, "Evaluation of statistical variability in 32 and 22 nm technology generation LSTP MOSFETs," *Solid-State Electron*. 54 , 767, 2010.

[64] N. Bandyopadhyay, Y. Bai, B. Gokden, A. Myzaferi, S. Tsao, S. Slivken, and M. Razeghi., "Watt level performance of quantum cascade lasers in room temperature continuous wave operation at $\lambda \sim 3.76$ μm," *Appl. Phys. Lett*. 97, 131117, 2010.

[65] N. Bandyopadhyay, S. Slivken, Y. Bai, and M. Razeghi, "High power, continuous wave, room temperature operation of $\lambda \sim 3.4$ μm and $\lambda \sim 3.55$ μm InP-based quantum cascade lasers," *Appl. Phys. Lett*. 100, 212104, 2012.

[66] M. Wienold, M. P. Semtsiv, I. Bayrakli, W. T. Masselink, M. Ziegler, K. Kennedy, and R. Hogg, "Optical and thermal characteristics of narrow-ridge quantum-cascade lasers," *J. Appl. Phys*. 103, 083113, 2008.

[67] B. Abeles, D. S. Beers, G. D. Cody, and J. P. Dismukes, "Thermal conductivity of Ge-Si alloys at high temperatures," *Phys. Rev.* 125, 44, 1962.

[68] C. J. Foss and Z. Aksamija, "Strain effects on thermal transport and anisotropy in thin-films of Si and Ge," *J. Appl. Phys.* 120, 225104, 2016.

[69] Paolo Giannozzi et al., "QUANTUM ESPRESSO: a modular and open-source software project for quantum simulations of materials," *J. Phys.: Condens. Matter.* 21, 395502, 2009.

[70] Y. B. Shi and I. Knezevic, "Nonequilibrium phonon effects in midinfrared quantum cascade lasers," *J. Appl. Phys.* 116, 123105, 2014.

[71] Y. Bai, N. Bandyopadhyay, S. Tsao, S. Slivken, and M. Razeghi, "Room temperature quantum cascade lasers with 27% wall plug efficiency," *Appl. Phys. Lett.* 98, 181102, 2011.

[72] Y. Bai, S. Darvish, S. R. Darvish, S. Slivken, W. Zhang, A. Evans, J. Nguyen, and M. Razeghi, "Room temperature continuous wave operation of quantum cascade lasers with watt-level optical power," *Appl. Phys. Lett.* 92(10), 101105, 2008.

[73] A. Lyakh, R. Maulini, A. Tsekoun, R. Go, S. Von der Porten, C. Pflügl, L. Diehl, Federico Capasso, and C. Kumar N. Patel, "High-performance continuous-wave room temperature 4.0-μm quantum cascade lasers with single-facet optical emission exceeding 2 W," *PNAS*, 107, 18799–18802, 2010.

[74] N. Bandyopadhyay, Y. Bai, S. Tsao, S. Nida, S. Slivken, and M. Razeghi, "Room temperature continuous wave operation of $\lambda \sim 3$-3.2 μm quantum cascade lasers," *Appl. Phys. Lett.* 101, 241110, 2012.

[75] Y. B. Shi, S. Mei, O. Jonasson, and I. Knezevic, "Modeling quantum cascade lasers: Coupled electron and phonon transport far from equilibrium and across disparate spatial scales," Fortschritte der Physik - Progress of Physics, 1600084 (2016) / DOI 10.1002/prop.201600084 https://dx.doi.org/10.1002/prop.201600084

[76] H. Page, C. Becker, A. Robertson, G. Glastre, V. Ortiz, and C. Sirtori, "300 K operation of a GaAs-based quantum-cascade laser at $\lambda \approx 9$ μm," *Appl. Phys. Lett.* 78, 3529, 2001.

[77] Q. Zhang, F.-Q. Liu, W. Zhang, Q. Lu, L. Wang, L. Li, and Z. Wang, "Thermal induced facet destructive feature of quantum cascade lasers," *Appl. Phys. Lett.* 96, 141117, 2010.

[78] O. Jonasson, "Quantum Transport in Semiconductor Heterostructures Using the Wigner-Function and Density-Matrix Formalisms," Ph.D. dissertation, Department of Physics, Univ. Wisconsin, Madison, 2016.